Importance of electron time-of-flight measurements in momentum imaging of saddle-point electron emission

Victor D. Irby

Department of Physics, University of South Alabama, Mobile, Alabama 36688-0002

Over the past several years, another type of spectrometer has been developed that proves to be superior to conventional spectrometers. In this ''momentum imaging'' spectrometer, electrons and target-recoil ions produced in ionizing collisions are accelerated to opposing position-sensitive detectors by an external electric field. The momentum imaging spectrometer essentially projects (or images) the initial three-dimensional (3D) electron and recoil-ion momentum vectors onto the 2D plane of each corresponding detector. Because the spread in electron arrival time is quite small in comparison with the spread in recoil-ion arrival time, one can utilize the electron signal as a timing marker to extract the full 3D momentum vector of the recoiling ion. This technique has proven to be quite successful in cold-target recoil-ion momentum spectroscopy. Momentum imaging methods have also been recently utilized in the search for evidence of saddle-point electron emission. Experimental studies of H^+ and He^{2+} incident on He were carried out by Abdallah *et al.* [Phys. Rev. A **56**, 2000 (1997)]. Rather surprisingly, their results exhibited projectile-charge dependent shifts *in the opposite direction* than that implied by the saddle-point mechanism. However, as we shall demonstrate, proper saddle-point shifts may be observed if one takes into account the time of flight of the electron. [S1050-2947(99)04308-5]

INTRODUCTION

The single ionization of a neutral atom by a fast projectile of charge Q_p can occur through two separate dynamical processes. In one process, the electron is removed from the target and freely emerges from the collision, leaving behind a target ion of charge $Q_t = 1$ while the projectile charge Q_p remains unchanged. In the second process, the electron is not only removed from the target, but is also captured by the projectile, reducing the projectile charge by one. In this paper, we will refer to the first process as *single ionization*, and the second process as *single capture*.

Experimental studies have shown that ionization of a neutral atom is dominated by the single-capture process at incident projectile velocities lower than the average orbital speed of the target electron. In contrast, single-ionization (free electron release) becomes dominant at projectile velocities exceeding the target-electron orbital speeds. While the process of single-capture is fairly well understood, there still exists many questions as to the actual mechanisms involved in the single-ionization process.

Over the past decade, a description of a possible mechanism involved in the single-ionization process termed ''saddle-point ionization'' has emerged. However, this saddle-point model has been the subject of much debate and continues to generate controversy.

The saddle-point mechanism was first suggested by Olson [1]. As the charged projectile approaches the target atom, the potential well initially entrapping the electron begins to merge with the potential well of the projectile, forming a transitory ''saddle point'' (or equiforce position) along the line separating the two ions. As the projectile begins to recede from the target ion, the electron may escape capture by the projectile and recapture by the target ion by becoming stranded on or near the saddle point of the collision system. The velocity, $\vec{v}_s$, at which the saddle point travels is given by

$$\vec{v}_s = \frac{\vec{v}_p}{1 + \sqrt{\dfrac{Q_p}{Q_t}}}, \tag{1}$$

where $\vec{v}_p$ is the projectile velocity. A classical description of single ionization, based on the concept of saddle-point electrons, was introduced by Irby [2]. Using this simple picture, Irby was able to derive scaling equations for the maximum in total single-ionization cross sections, and the projectile energies at where they occur, that are in excellent agreement with previously existing empirical scaling laws [3].

One of the first experimental searches for saddle-point electrons was carried out by Olson *et al.* [4]. Their results, for H^+ incident on He, indicated that a large fraction of electrons were emitted at speeds half that of the projectile. More convincing experiments of Irby *et al.* [5] and Gay *et al.* [6], for H^+ and He^{2+} incident on He, exhibited projectile-charge dependent shifts of the maximum in electron energy spectra in correspondence with Eq. 1. However, in direct contrast, experimental results of Bernardi *et al.* [7,8] and Dubois [9] did not exhibit such projectile-charge dependent shifts. The cause of the disagreement among the measurements eluded investigators and was the subject of much discussion.

One recent explanation of the disparity among the measurements was proposed by Irby *et al.* [10–12]. It was suggested that electron plate-impact contamination within individual analyzers could obscure low-energy electron spectra, subsequently washing out evidence of saddle-point shifts.
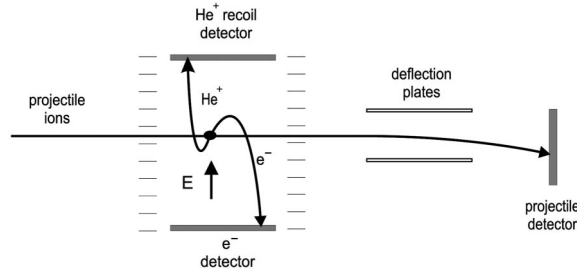
FIG. 1. Schematic of electron momentum imaging spectrometer.

More recently, Rudd [13] demonstrated that plate-impact contamination could account for ''filling in of the minimum'' of particular electron spectra involving electron projectiles, and also account for discrepancies among measurements (other than saddle-point type) made by many different investigators.

Most researchers involved in electron spectroscopy now agree that proper experimental techniques are required to eliminate spectral contamination caused by electrons impacting electrode plates or any other surfaces within a spectrometer. In addition, the majority of investigators also agree that measurements should involve proper coincidence techniques. Many earlier measurements involved detection of only electrons, from ion-atom collisions, and could not distinguish between separate collision channels. Thus, over the past several years, another type of electron spectrometer has been developed which overcomes many of the experimental problems researchers have encountered in the past.

A schematic diagram illustrating the basic principles of the spectrometer is shown in Fig. 1. The electron momentum imaging (EMI) spectrometer utilizes two-dimensional position-sensitive detectors (microchannel plates) that are placed in a uniform electric field (E). The E-field is perpendicular to the incident ion beam. Ionized electrons are generated at the intersection of the ion beam and the effusive gas target. Since both electrons and target/recoil ions are generated within the E-field, they are accelerated to opposing two-dimensional (2D) detectors. Projectile ions are also collected onto a separate 2D microchannel plate. The detector-impact position of an ejected electron is proportional to its corresponding component of momentum. Hence, the detected impact positions are essentially an ''image'' of the electron's momentum components. Thus, the spectrometer is referred to as a momentum imaging device. For a comprehensive overview of momentum imaging spectrometers, an excellent review article is given by Ullrich *et al.* [14].

The EMI spectrometer has several advantages over conventional types of spectrometers. The overall detection efficiency, for both electrons and recoils, is on the order of 100% since essentially all the particles emitted in the collision can be collected onto the detectors. Also, plate-impact contamination is virtually nonexistent. Finally, since both position and timing signals can be extracted from the 2D microchannel plate detectors, collision products can be measured in coincidence. Thus, the EMI spectrometer proves to be superior to conventional spectrometers.

Researchers have recently utilized EMI spectrometers in the search for evidence of saddle-point electrons. Experimental studies of H^+, He^{2+}, and carbon ions incident on He were carried out by Abdallah *et al.* [15]. Rather surprisingly,
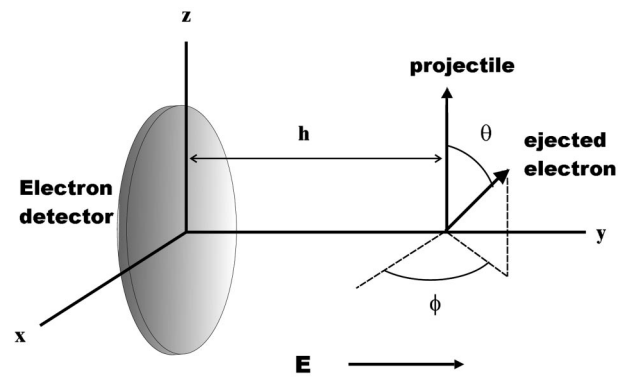

FIG. 2. Collision coordinates. Electric field is directed along the positive *y* axis.

their results for H^+ and He^{2+} ions exhibited projectile-charge dependent shifts *in the opposite direction* than that implied by Eq. (1). These ''antisaddle'' shifts certainly seem to contradict the saddle-point hypothesis. However, as we shall demonstrate below, the antisaddle shifts observed by Abdallah *et al.* can be construed as an experimental artifact, that arises from lack of complete knowledge of all kinematic parameters necessary in the data analysis. We will show that saddle-point shifts may be observed if one takes into account the time of flight of the electron.

COMPUTER SIMULATIONS OF EMI SPECTROMETER

In order to demonstrate the necessity of measuring the electron time of flight in studies involving electron momentum imaging, we have performed computer simulations and calculations using Sigma Plot computer graphics program [16]. The coordinates used in these calculations are illustrated in Fig. 2. The *z*-axis is oriented along the direction of the incident projectile ions. The electron is ejected at a distance $y=h$ from the detector at $x=z=0$. For a uniform electric field, the position at which an electron impacts the detector is given by

$$y = 0, \tag{2a}$$

$$x = v \sin\theta \cos\phi\, t_f, \tag{2b}$$

$$z = v \cos\theta\, t_f, \tag{2c}$$

$$t_f = \frac{v \sin\theta \sin\phi}{a} + \sqrt{\left\{\frac{v \sin\theta \sin\phi}{a}\right\}^2 + \frac{2h}{a}}, \tag{2d}$$

where θ is the electron ejection angle, ϕ is the azimuthal angle, v is the ejection speed, t_f is the time of flight, and a is the acceleration ($a = eE/m_e$). Utilizing Sigma Plot's math transforms, 5000 electrons were generated with random v, θ, and ϕ, and the detector impact positions were calculated from Eq. (2). More specifically, the electron-ejection speeds, v, were generated from a random Gaussian distribution centered at $v=1$ a.u. The central peak of the distribution ($v_{max}=1$ a.u.) was chosen to simulate saddle-point electrons emitted by singly-charged projectiles traveling at $v_p=2$ a.u. ($Q_t=1$). A histogram of a typical electron speed distribution
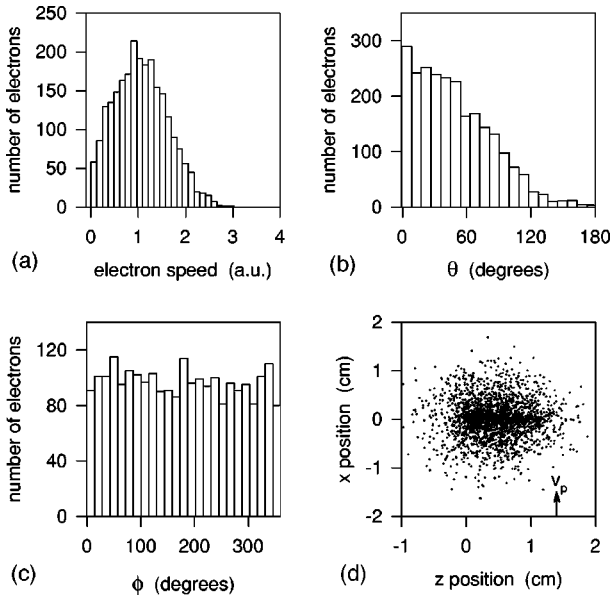
FIG. 3. (a) Initial electron speed distribution. Parameters used are $v_{max}=1.0$ a.u. and $\Delta v=0.6$ a.u. (b) Initial distribution of electron ejection angles. Parameters used were $\Delta\theta=60°$. (c) Distribution of azimuthal ejection angles. (d) Scatter plot of electron detector impact positions. The arrow illustrates the z position for an electron emitted at $v_e=v_p$ and $\theta=0$.
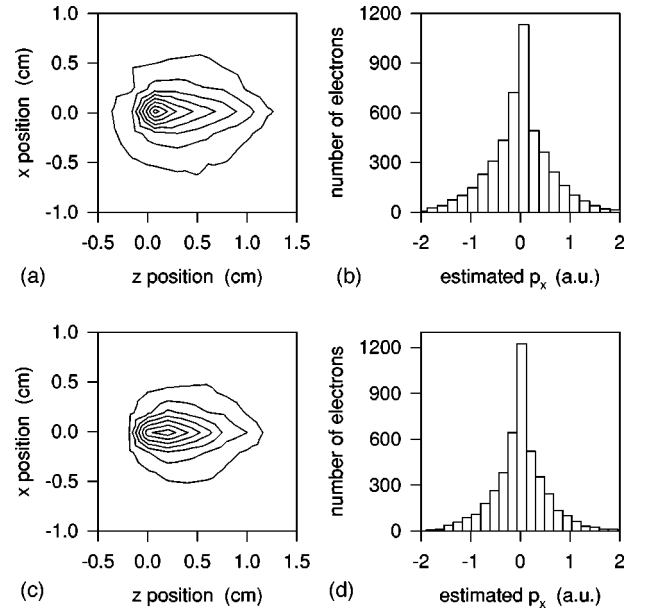

FIG. 4. (a) Contour plot of electron impact positions for H^+ projectiles. Parameters used are $v_{max}=1.0$ a.u., $\Delta v=0.6$ a.u., and $\Delta\theta=75°$. (b) Estimated x-momentum distribution (H^+) for constant time of flight $t_f=3.2$ ns. (c) Contour plot of electron impact positions for He^{2+} projectiles. Parameters used are $v_{max}=0.828$ a.u., $\Delta v=0.6$ a.u., and $\Delta\theta=60°$. (d) Estimated x-momentum distribution (He^{2+}) for constant time of flight $t_f=3.2$ ns.

is illustrated in Fig. 3(a) for a half-width half-maximum (HWHM), Δv, equal to 0.6 a.u. Electron ejection angles, θ, were generated in a similar fashion and are illustrated in Fig. 3(b) for a HWHM of $\Delta\theta=60°$. A random uniform distribution was used for the azimuthal angle ϕ [see Fig. 3(c)]. The electron impact positions were then calculated for $h=0.038$ m and an electric field of $E=420$ V/cm, which correspond to the experimental parameters reported by Abdallah *et al.* [15] and Kravis *et al.* [17]. (In the random-generation sequence, both positive and negative values of θ and v were obtained. To avoid any confusion, all electron shots with $\theta<0$ and $v<0$ were discarded. Thus, the total number of electron shots illustrated in Fig. 3 is about 2500.) The arrow in Fig. 3(d) illustrates the z-position for an electron emitted at $v_e=v_p$ and $\theta=0$.

Sigma Plot simulations were performed for proton and alpha particles incident on helium. The parameters Δv and $\Delta\theta$ were adjusted to obtain qualitative agreement with the experimental data of Abdallah *et al.* [15]. Contour plots of electron detector-impact positions are illustrated in Figs. 4(a) and 4(c) for an approximate total of 5000 electrons. In Fig. 4(a), the parameters used were $v_{max}=1$ a.u, $\Delta v=0.6$ a.u., and $\Delta\theta=75°$. To simulate alpha particle projectiles, parameters were chosen as $v_{max}=0.828$ a.u, $\Delta v=0.6$ a.u., and $\Delta\theta=60°$. One may argue that the chosen angular distributions may be too large. However, estimates of transverse momentum, p_x, given in Figs. 4(b) and 4(d) are in reasonable agreement with data of Abdallah *et al.* (in fact the angular distributions may be somewhat underestimated). The momentum distributions shown in Figs. 4(b) and 4(d) were obtained by using Eq. (2) and assuming, as in the data analysis of Abdallah *et al.*, a constant time of flight 3.2 ns. (This time of flight is chosen on the assumption that the transverse velocity, v_y, of the electron is small. The spread in electron

arrival time, resulting from transverse ejection speeds, is typically much less than 1.0 ns.)

As one can see from Figs. 4(a) and 4(c), the simulations presented here exhibit an antisaddle shift similar to that observed by Abdallah *et al.* [15]. This can be seen more clearly by estimates of the longitudinal momentum, p_z, obtained by using a constant time of flight $t_f=3.2$ ns, and are shown in Figs. 5(a) and 5(c). In order to examine electrons emitted at small ejection angles θ, longitudinal momenta p_z were also calculated for a small slice through the x-position axis. The small angle p_z obtained, for $|x|\leqslant0.04$ cm, are illustrated in Figs. 5(b) and 5(d). Again, the calculations exhibit an antisaddle shift, despite the fact that the initial distributions were chosen so as to simulate saddle-point electrons.

The antisaddle shift observed in these simulations arises from trying to estimate p_z without complete knowledge of all the kinematic variables. From examination of Eq. (2), it is clear that there are three equations and four unknowns (the measured quantities are x, z, and $y=0$, and the unknowns are v_x, v_y, v_z, and t_f). Thus, in order to obtain even one component of ejection velocity, one *must* measure the time of flight along with detector-impact position. Unfortunately, due to a limiting time resolution of 1 ns, Abdallah *et al.* [15] were unable to measure the time of flight of the electrons in their work. However, in these simulations, we have the luxury of knowing both the detector-impact position and the time of flight. Electron time-of-flight distributions for the simulated proton and alpha collisions are illustrated in Figs. 6(a) and 6(c).

In order to observe true saddle-point shifts, we must examine only those electrons that are emitted at small ejection angles. (In earlier experimental work of Irby *et al.* [5,10], it was reported that saddle-point shifts were observed only at
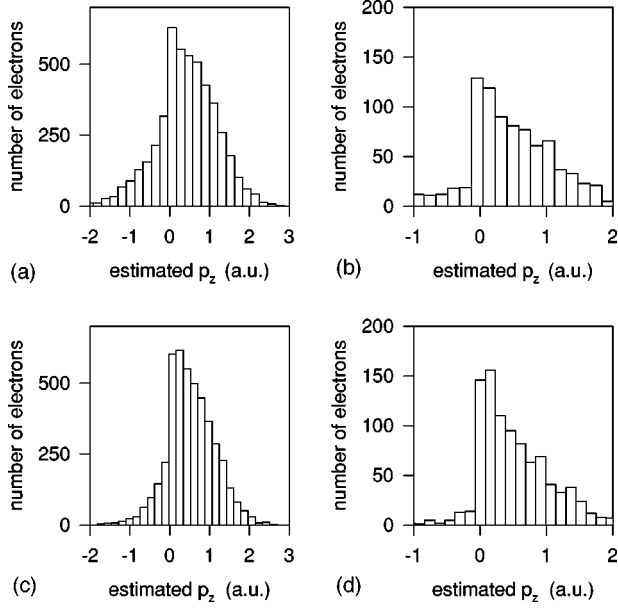
FIG. 5. (a) Estimated z-momentum distribution (H^+) for constant time of flight $t_f = 3.2$ ns. (b) Estimated z-momentum distribution (H^+) for small angle emission (see text). (c) Estimated z-momentum distribution (He^{2+}) for constant time of flight $t_f = 3.2$ ns. (d) Estimated z-momentum distribution (He^{2+}) for small angle emission (see text).

angles less than 20°.) Utilizing Eq. (2) and the electron time of flight, we can then select only those electrons whose emission angles are less than 15°. This can be accomplished by choosing electron detector-impact positions that satisfy the relation

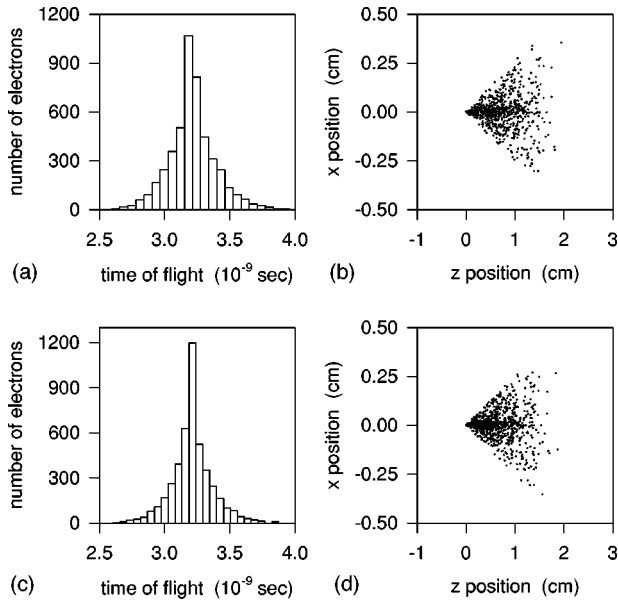$$\frac{z}{t_f\sqrt{v_x^2 + v_y^2 + v_z^2}} \geq \cos 15°, \qquad (3)$$

FIG. 6. (a) Electron time-of-flight distribution for H^+ projectiles. (b) Scatter plot of electron detector-impact positions (H^+) for $\theta \leq 15°$. (c) Electron time-of-flight distribution for He^{2+} projectiles. (d) Scatter plot of electron detector-impact positions (He^{2+}) for $\theta \leq 15°$.
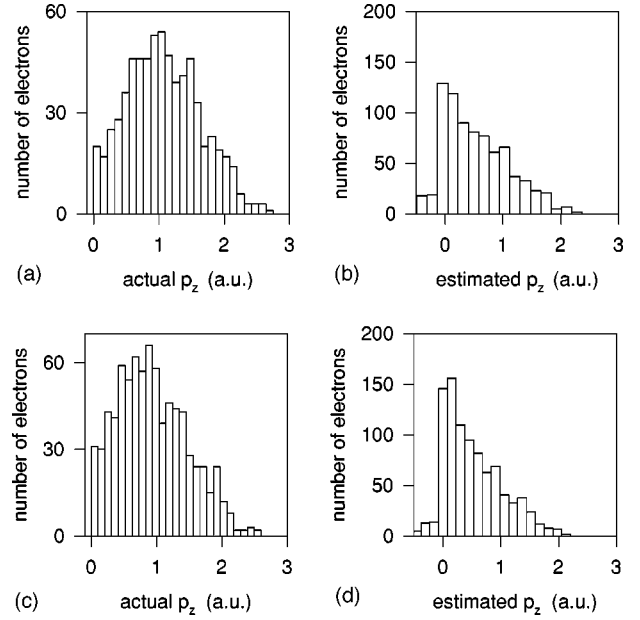

FIG. 7. (a) Actual z-momentum distribution (H^+) for $\theta \leq 15°$. (b) Estimated z-momentum distribution (H^+) for small angle emission. (c) Actual z-momentum distribution (He^{2+}) for $\theta \leq 15°$. (d) Estimated z-momentum distribution (He^{2+}) for small angle emission.

where the velocity components are obtained from the detector-impact position and time of flight:

$$v_x = \frac{x}{t_f}, \qquad (4a)$$

$$v_z = \frac{z}{t_f}, \qquad (4b)$$

$$v_y = \frac{1}{2}at_f - \frac{h}{t_f}. \qquad (4c)$$

Scatter plots for electrons emitted at $\theta \leq 15°$ [obtained from Eqs. (3) and (4)] are presented in Figs. 6(b) and 6(d). The number of electrons shown in Figs. 6(b) and 6(d) account for 20% of the total used in the simulation. Selecting only these electrons, we then compute the *actual* longitudinal momentum p_z, using the known t_f's, and present them in Figs. 7(a) and 7(c). The estimated small-angle p_z, from Figs. 5(b) and 5(d), are also replotted in Figs. 7(b) and 7(d) for comparison. One can readily see how the electron time of flight affects the data analysis.

Figures 6(b) and 6(d) seem to suggest that a better estimate of p_z, for data that does *not* include time of flight measurements, can be obtained by selecting only electrons that satisfy

$$\frac{|x|}{z} \leq \tan 15° \qquad (5)$$

(using only positive z-impact positions). However, electrons that are emitted at $\theta > 15°$ will be accidentally counted in this analysis if their azimuthal angle ϕ is greater than zero.

This follows from the fact that $x/z = \tan \theta$ only for $\phi = 0$ [see Eq. (2)]. To be more precise, let us assume that the actual ejection angle θ is greater than $15°$. If

$$\tan \theta \cos \phi \leq \tan 15° \qquad (6)$$

then the electron will be erroneously counted as being emitted at $\theta \leq 15°$. (In this simulation, this type of analysis overestimates the number of electrons by a factor of 1.5).

CONCLUSIONS

As we have thus shown, utilizing the above computer simulations, electron time-of-flight measurements can be crucial in the proper analysis of momentum-imaging spectra involving electrons. In addition, the above results also indicate that saddle-point ionization should not be completely ruled out as a viable mechanism involved in the production of freely-emerging electrons in singly-ionizing collisions.

However, these results should not distract from the importance of and advances made by momentum-imaging spectrometry. We also feel that the innovative and already pioneering techniques of momentum-imaging can be taken one step further, by pursuing better timing resolution. The combination of electron momentum-imaging spectrometry with picosecond timing, for instance, could enable researchers to observe the interactions between charged particles with detail possibly never seen before, greatly enhancing our understanding of the dynamical nature of ion-atom collisions.

[1] R. E. Olson, Phys. Rev. A **27**, 1871 (1983).

[2] V. D. Irby, Phys. Rev. A **39**, 54 (1989).

[3] R. A. Phaneuf, R. K. Janev, and M. S. Pindzola, Oak Ridge National Laboratory Report No. ORNL-6090/V5 (Controlled Fusion Atomic Data Center, Oak Ridge, TN 1987) (unpublished).

[4] R. E. Olson, T. J. Gay, H. G. Berry, E. B. Hale, and V. D. Irby, Phys. Rev. Lett. **59**, 36 (1987).

[5] V. D. Irby, T. J. Gay, J. Wm. Edwards, E. B. Hale, M. L. McKenzie, and R. E. Olson, Phys. Rev. A **37**, 3612 (1988).

[6] T. J. Gay, M. W. Gealy, and M. E. Rudd, J. Phys. B **23**, L823 (1990).

[7] G. Bernardi, S. Suàrez, P. D. Fainstein, C. R. Garibotti, W. Meckbach, and P. Focke, Phys. Rev. A **40**, 6863 (1989).

[8] G. Bernardi, P. Fainstein, C. R. Garibotti, and S. Suàrez, J. Phys. B **23**, L139 (1990).

[9] R. D. DuBois, Phys. Rev. A **48**, 1123 (1993).

[10] V. D. Irby, S. Datz, P. F. Dittner, N. L. Jones, H. F. Krause, and C. R. Vane, Phys. Rev. A **47**, 2957 (1993).

[11] V. D. Irby, Phys. Rev. A **51**, 1713 (1995).

[12] V. D. Irby, in *Two-Center Effects in Ion-Atom Collisions*, edited by T. J. Gay and A. F. Starace (American Institute of Physics, New York, 1996), p. 237.

[13] M. E. Rudd, Rev. Sci. Instrum. **68**, 3014 (1997).

[14] J. Ullrich, R. Moshammer, R. Dörner, O. Jagutzki, V. Mergel, H. Schmidt-Böcking, and L. Spielberger, J. Phys. B **30**, 2917 (1997).

[15] M. D. Abdallah, S. Kravis, C. L. Cocke, Y. Wang, V. D. Rodriguez, and M. Stöckli, Phys. Rev. A **56**, 2000 (1997).

[16] SigmaPlot for Windows, version 2.01, SPSS Inc., Chicago, IL.

[17] S. D. Kravis, M. Abdallah, C. L. Cocke, C. D. Lin, M. Stöckli, B. Walch, and Y. D. Wang, Phys. Rev. A **54**, 1394 (1996).